New magnetic phase and magnetic coherence in Nd/Sm(001) superlattices

2006 J. Phys.: Condens. Matter 18 4995

(http://iopscience.iop.org/0953-8984/18/22/001)

INSTITUTE OF PHYSICS PUBLISHING JOURNAL OF PHYSICS: CONDENSED MATTER

J. Phys.: Condens. Matter **18** (2006) 4995–5016 doi:10.1088/0953-8984/18/22/001

New magnetic phase and magnetic coherence in Nd/Sm(001) superlattices

S Soriano[1,2], C Dufour[1], K Dumesnil[1] and A Stunault[3]

[1] Laboratoire de Physique des Matériaux, Université H. Poincaré-Nancy I, BP 239, 54506 Vandoeuvre les Nancy cedex, France
[2] Universidade Federal do Rio de Janeiro, Instituto de Física, 21945-970, Rio de Janeiro-RJ, Brazil
[3] ILL, BP 156X, 38042 Grenoble cedex, France

Received 5 December 2005, in final form 31 January 2006
Published 16 May 2006
Online at stacks.iop.org/JPhysCM/18/4995

Abstract

In order to investigate magnetic phenomena in Nd and Sm layers separately, resonant x-ray magnetic scattering experiments have been performed to study Nd/Sm(001) superlattices with different relative layers thickness. The samples were grown using molecular beam epitaxy, and optimized to yield dhcp Sm growth and thus a *coherent* dhcp stacking across the Nd/Sm superlattices. The magnetic phases in Sm layers are very close to the ones evidenced in dhcp thick films. In contrast, the magnetism in Nd layers shows strong differences with the bulk case. In superlattices with a large Sm thickness (>8 nm), no magnetic scattering usually associated with Nd magnetic structure was detected. In superlattices with smaller Sm thickness (<4 nm), new Nd magnetic phases have been observed. A detailed analysis of the propagation of the magnetic structures in the cubic and hexagonal sublattices of both Sm and Nd is presented. Both Sm hexagonal and cubic magnetic phases propagate coherently through 3.7 nm thick Nd layers but remain confined in Sm layers when the Nd layers are 7.1 nm thick. In contrast, the critical Sm thickness allowing a coherent propagation of Nd magnetic order is different for the hexagonal and cubic sublattices above 5 K. Finally, we show that: (i) a spin-density wave and a 4f magnetic order with perpendicular polarization are exclusive *on a given crystallographic site* (either hexagonal or cubic); (ii) a 4f magnetic order *on a crystallographic site* does not perturb the establishment of a spin-density wave with a perpendicular polarization *on the other site*.

1. Introduction

The study of the magnetic properties of pure rare-earth metals at the nanometric scale is of interest for a better understanding of rare earth magnetism and also of rare earth based nanostructures. Rare-earth intermetallics, for example, are challenging materials to be

integrated in nanoscales devices, due to their properties as permanent magnets, magnetostrictive sensors, perpendicular magnetic recording media, and so on.

In lanthanide elements, the combination of weak exchange and anomalous large crystal field and magnetostrictive interactions, arising from the strong spin–orbit coupling and the highly non-spherical 4f charge distribution, results in comparable magnitude for exchange and crystal field energies. This situation, as well as the long-range and oscillating character of the indirect exchange interaction, leads to a large number of exotic modulated structures. Since the discovery of the propagation of magnetic order through nonmagnetic spacer layers [1], the study of rare-earth superlattices has been shown to provide a unique way of probing the nature of this exchange coupling in the rare-earth metallic state [2]. In non magnetic/magnetic superlattices, it is generally accepted that long-range order is established by the magnetic rare earth inducing a spin-density wave in the conduction band of the nonmagnetic element (the (5d, 6s) electrons), which then propagates the order to the next magnetic block. For example, in the case of helical order, the phase and the chirality of the helix are preserved from one magnetic layer to the other. From the experimental results obtained from numerous rare-earth superlattices [2], one can conclude that the propagation of a magnetic phase through a spacer layer is coherent if two conditions are fulfilled:

- the crystallographic structures of the constituents are similar and coherent over the superlattice, and
- the thickness of the spacer is smaller than a critical thickness; its value varies in general between 8 and 12 nm, depending on the superlattice.

To date most work on rare-earth superlattices has concerned hcp heavy rare-earth metals [1–6]. Following the pioneering works on Gd/Y [1] and Dy/Y [3], superlattices with several non-magnetic spacers have been grown (Lu [6], Sc [7]). Subsequently, magnetic/magnetic heavy rare-earth superlattices were investigated and competition effect between the magnetic structures was observed [8–10]. Of some relevance to the present work are the behaviours of Dy/Er [8], Ho/Er [9] and Ho/Tm [10] superlattices. For these superlattices, there is a competition between the ordering along the **c**-axis and the ordering in the basal plane, so that, in a given layer, a spin-density wave and a magnetic order with perpendicular polarization are exclusive.

Recently, studies have been carried out on superlattices combining two light rare-earth metals (Nd/La [11], Nd/Pr [12, 13] and Ce/Nd [14]), where both constituents have a dhcp structure, with sublattices of two crystallographic sites with hexagonal and cubic local symmetry. In Nd/Pr and Nd/La, the magnetic ordering of Nd is qualitatively similar to that of bulk Nd metal. In all studies, the Nd hexagonal sites ordering propagates coherently through several bilayers, whereas the magnetic order of the cubic sublattice is confined to individual blocks or is suppressed. Furthermore, in Nd/Pr, an induced spin-density wave in the hexagonal sublattice of the Pr layers was observed. In Ce/Nd superlattices, the Nd and Ce magnetic orders appear to be mutually exclusive: in the samples with the thicker Nd layers, the magnetic structure is similar to that observed in Nd under applied pressure, with in-plane incommensurate magnetic order in the hexagonal sublattice and **c**-axis ferromagnetism in the cubic sublattice; in the sample with thickest Ce layers a magnetic structure similar to bulk β-Ce is observed.

Superlattices based on dhcp Sm and Nd are expected to lead to an even deeper understanding of the equilibrium between the leading interactions in rare-earth systems, because of two main features:

(i) each rare earth is dhcp and presents two different sublattices of crystallographic sites with different symmetries and magnetic orders, and

(ii) Sm and Nd exhibit competing crystal field anisotropies: the localized 4f moments in bulk Nd are mainly located in the basal plane, whereas moments in thick Sm dhcp films are aligned along the *c*-direction.

Moreover, it has been shown that, taking advantage of the possibility to grow dhcp Sm, *coherent* dhcp Nd/Sm superlattices can be elaborated by molecular beam epitaxy (MBE) [15]. As already emphasized, crystalline coherence is a necessary condition to observe magnetic coherence.

This paper is devoted to the determination of the magnetic phases in Sm and Nd layers, as well as to a study of their magnetic coherence, for a set of Nd/Sm superlattices with different relative thicknesses using resonant x-ray magnetic scattering (RXMS). RXMS has several advantages over more traditional neutron diffraction, and is able to provide unique insight into the magnetic ordering in epitaxial systems. First, by tuning to absorption edges, the magnetism of the different components may be studied separately. Then, the energy dependence of the magnetic scattering provides spectroscopic information on the magnetically ordered species. Furthermore, taking advantage of the different polarization dependence of the RXMS and Thomson charge scattering, one can drastically improve the signal-to-background ratio, which is of crucial importance for epitaxial samples, with small volumes of magnetic material. Finally, the superior wavevector resolution allows a more detailed study of incommensurate magnetic structures and of their coherence through superlattices.

The paper is organized as follows. Section 2 presents the experimental details: preparation of the single-crystal superlattices by MBE, description of standard x-ray and RXMS experimental set-up. The structural properties are described in section 3. The main results, i.e. the magnetic structures, their thermal evolution and their propagation, are presented in section 4 and discussed in section 5. Finally, some conclusions are drawn in section 6.

2. Experimental details

The samples were prepared by MBE in a vacuum chamber with base pressure $\approx 4 \times 10^{-11}$ Torr. They were grown on a (110) sapphire substrate, previously submitted to an ultrasonic treatment in a degreasing solution and then heated to 850 °C for one hour in the growth chamber. Following the method proposed by Kwo *et al* [16], the substrate was first covered by a 50 nm niobium buffer deposited at 800 °C. Samarium and neodymium were then evaporated from an effusion cell and an electron gun, respectively, and deposited onto the substrate kept in the 320–370 °C temperature range, in order to allow surface mobility while limiting interfacial interdiffusion. The deposition rate, calibrated using a quartz crystal monitor and an optical sensor, was of 0.05 nm s^{-1} and the pressure during evaporation process was around 10^{-9} Torr. There was no delay between the deposition of samarium and neodymium during the superlattice elaboration process. A 50 nm thick niobium layer finally covered the sample, in order to avoid further oxidation of the reactive light rare earth.

Preliminary structural analysis of the superlattices was performed using a high-resolution diffractometer equipped with a four-crystal monochromator. The diffraction patterns were obtained with the Kα wavelength of cobalt (1.7889 Å). The instrumental resolution of the diffractometer was 0.0005 $Å^{-1}$.

RXMS takes advantage of the enhancement of the elastic magnetic scattering cross section when the incident photon energy is tuned through an appropriate absorption edge of the studied element. The magnetic scattering arises from electric multipole transitions between core levels and unoccupied spin-polarized electronic states. The amplitude is related to the

spin-polarization and spin–orbit splitting of intermediate excited states and the overlap of the electronic orbitals of the initial (and final) and the excited state [17].

The RXMS experiments were performed at the ID20 and BM28 beamlines of the European Synchrotron Radiation Facility. The incoming flux on the sample was of the order of 10^{13} ph s^{-1} at the maximum ring current of 200 mA on the undulator beamline ID20, and 10^{11} ph s^{-1} on the bending magnet beamline BM28, equipped for our experiments with two short flat Si mirrors for harmonics rejection. On ID20, the undulator source ensures a high degree of incident linear polarization in the horizontal plane, >99%, and the energy resolution was ≈0.7 eV at 6.7 keV. At the bending magnet beamline XMaS (BM28), the degree of linear polarization depends critically on the vertical opening of the primary slits before the monochromator. It is 99.5% in the plane of the electron ring, but degrades quickly with the vertical opening of the primary slits. Our compromise was a slit opening of 1.5 mm (vertical beam divergence 63 mrad), that cuts about 1/2 of the photon flux, but gives a degree of linear polarization of 95%, with an energy resolution ≈1.7 eV at 6.7 keV.

On ID20, the samples were mounted in an Orange cryostat (1.5–300 K), with $\mathbf{a}^*$ and $\mathbf{c}^*$ in the horizontal scattering plane. On BM28, we used a helium closed-cycle refrigerator, with a Joule–Thomson third stage (base temperature 1.8 K), and the scattering plane was vertical.

Using the conventional notations σ and π for photon beam polarization perpendicular and parallel to the scattering plane, respectively, we note that for pure incident polarization the Thomson charge scattering is also pure incident $\sigma(\pi)$ polarized, while RXMS also involves rotated $\sigma - \pi$ $(\pi - \sigma)$ components. We took advantage of this feature by using a single-crystal polarization analyser on the scattered beam, and performing all RXMS measurements in the rotated channel, hence reducing the charge background from the substrate by several orders of magnitude. In addition to the separation of the two scattered polarization states, the analyser crystal filters out fluorescence photons which have energy several hundreds of eV below the absorption edge.

A Cu(220) analyser crystal, with a mosaic spread of 0.28° and a peak reflectivity of 3.5% at 6.7 keV, was used for polarization analysis at the Sm L_{III} and Nd L_{II} edges (6.716 and 6.722 keV, respectively). A LiF(220) crystal was used at the Nd L_{III} edge (7.312 keV). Its mosaic spread was of 0.14° and it showed a peak reflectivity of 10.4% at 6.2 keV.

Complementary studies were also performed in the un-rotated polarization channel, to characterize the chemical structure.

3. Structural characterization

For all superlattices, *in situ* reflection high-energy electron diffraction (RHEED) patterns collected after each Nd deposition and after each Sm deposition exhibit thin and continuous streaks. This reveals the single-crystal quality and the smoothness of the deposited layers.

As an example, patterns in figures 1(a) and (b) have been alternatively obtained every 30° after the deposition of $[Nd(7.1\ nm)/Sm(8.7\ nm)]_{33}$ (the last layer is a Sm one). The six-fold symmetry of the patterns, associated with the $\sqrt{3}$ ratio of the distance between the main streaks, show that the crystal surface structure is hexagonal and permit us to identify the **c**-axis as the rare-earth growth direction. The epitaxial relationships are

$$Al_2O_3(110) \parallel Nb(110) \parallel Nd(001) \parallel Sm(001)$$

with Nb[001] ∥ Nd[$\bar{1}$20] ∥ Sm[$\bar{1}$20] and Nb[$\bar{1}$10] ∥ Nd[100] ∥ Sm[100].

Both patterns in figure 1 exhibit satellite streaks, characteristic of an 11 × 11 surface reconstruction. This feature has been observed even for much thicker dhcp Sm films (several hundred nanometres) [15]. This is consistent with previous observations on Sm grown on

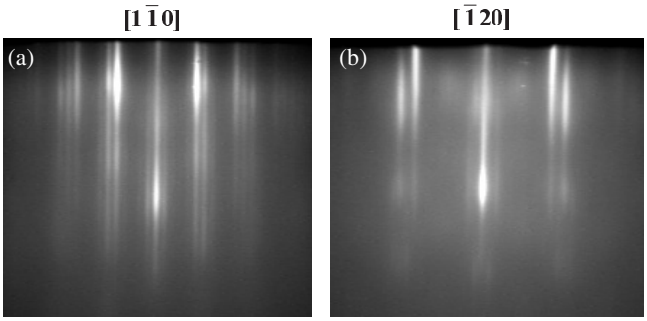

Figure 1. RHEED patterns obtained after the deposition of $[Nd(7.1\ nm)/Sm(8.7\ nm)]_{33}$ on Nb(110): (a) along the $[1\bar{1}0]$ rare-earth azimuthal directions; (b) along the $[\bar{1}20]$ rare-earth azimuthal directions.

Table 1. Superlattices structural parameters determined from x-ray diffraction.

	Periodicity (±0.2 nm)	c ($\pm 2 \times 10^{-3}$ Å)	Mosaicity (±0.01°)	Coherence length (±2 nm)	Crystal structure
$[Nd(3.7\ nm)/Sm(9.4\ nm)]_{43}$	13.1	11.7076	0.4	80	dhcp +'Sm'
$[Nd(7.1\ nm)/Sm(8.7\ nm)]_{33}$	15.8	11.740	0.32	87	dhcp
$[Nd(18.8\ nm)/Sm(3.7\ nm)]_{42}$	22.5	11.7816	0.15	155	dhcp
$[Nd(6.2\ nm)/Sm(3.7\ nm)]_{84}$	9.9	11.758	0.18	148	dhcp
$[Nd(15.4\ nm)/Sm(1.4\ nm)]_{43}$	16.8	11.79	0.16	140	dhcp

Mo(110) [18]. The surface reconstruction has been associated to a large (22%) expansion of the Sm atomic radius in the top monolayer Sm atoms, related to the divalent character of the Sm surface. The divalent atoms form a complex arrangement, incommensurate with the atomic arrangement present in the core of the Sm layer.

Table 1 summarizes the structural parameters of the superlattices presented here. The thickness of the individual Sm and Nd layers range from 1.4 to 18.8 nm. They have been deduced by combining x-ray diffraction (to obtain the chemical modulation) and microanalysis (to determine the stoichiometry of the bilayer).

The crystal structure and the coherence of the superlattices have been checked by x-ray diffraction. Using the usual hexagonal basis, with **c** (and $\mathbf{c}^*$) perpendicular to the hexagonal (**a**, **b**) plane, we have performed scans in the reciprocal space along the $[00L]$ and $[10L]$ directions [15]. Scans along $[00L]$ are presented in figure 2 for the whole set of superlattices. They exhibit an average main Bragg peak, indexed as (004), surrounded by satellites reflecting the periodicity of the superlattice. Depending on the sample, the structural coherence length deduced from the width of the main Bragg peak varies between 80 and 155 nm, and the mosaic spread deduced from a transverse scan through the (004) Bragg peak varies between 0.15° and 0.4° (table 1).

For the whole set of superlattices, the scan along $[10L]$ shows four Bragg peaks, indexed as (106), (107), (108) and (109), surrounded by several satellites. As an example, figure 3 presents this scan for the $[Nd(7.1\ nm)/Sm(8.7\ nm)]_{33}$ superlattice. The relative positions of the satellites correspond to the superperiodicity of 15.8 nm and the width of the peaks indicates that the structural coherence length of the dhcp stacking is about 48 nm. These results show that:

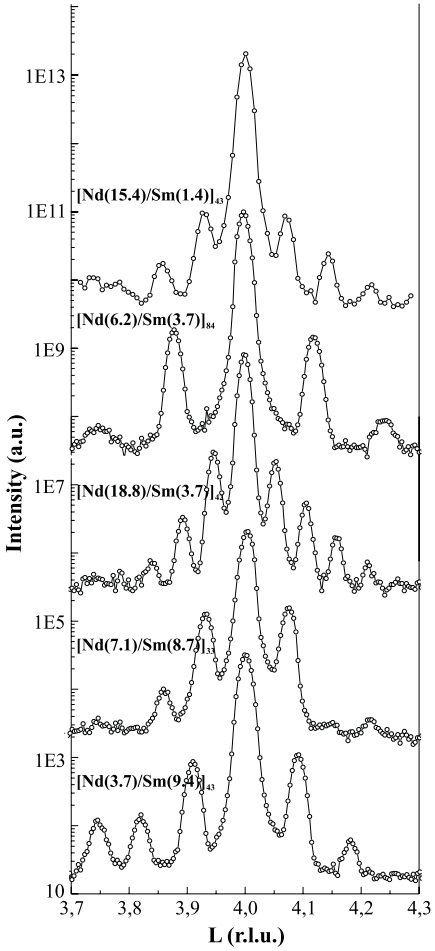

Figure 2. X-ray diffraction pattern measured with the momentum transfer parallel to [00L] for the whole set of superlattices. The x-axis is in reciprocal lattice units (rlu) of dhcp stacking. The curves have been offset vertically for clarity.

(i) both Sm and Nd layers present a dhcp stacking, and
(ii) the ABAC–ABAC–ABAC. . . sequence propagates from Sm to Nd and from Nd to Sm over approximately three bilayers, without stacking faults at the interfaces.

The superlattice exhibits a long-range dhcp structure with a coherence length of the ABAC alternation larger than the Nd/Sm superperiodicity. Similar results have been obtained for the other superlattices.

To summarize, the crystal structure is dhcp for all superlattices. However, note that for the superlattice [Nd(3.7 nm)/Sm(9.4 nm)]$_{43}$, a small amount of Sm exhibiting the 'Sm-structure' (Sm with the bulk-like nine-plane stacking sequence) is present, which is not exclusive of a coherent dhcp stacking. The presence of Sm with the 'Sm-structure' is generally observed in superlattices with thick Sm layers compared to the Nd ones, although it is not observed in thick dhcp Sm film (up to 1000 nm) deposited on a 2 nm Nd buffer. This is likely related to the lowering of the substrate temperature in the Nd/Sm superlattices, in order to avoid interdiffusion.

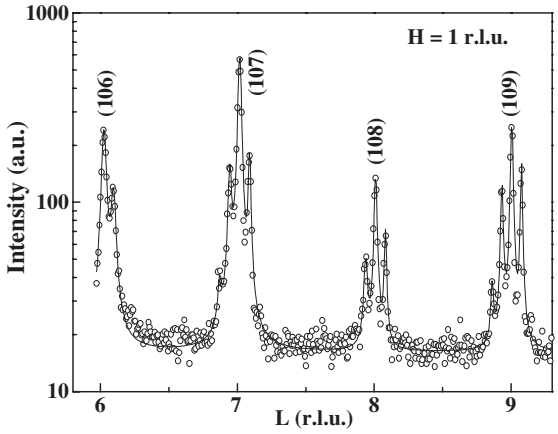

Figure 3. X-ray diffraction pattern measured with the momentum transfer parallel to [10L] for [Nd(7.1 nm)/Sm(8.7 nm)]$_{33}$. The x-axis is in reciprocal lattice units (rlu) of dhcp stacking.

The chemical interface between Sm and Nd has not been studied in detail for the Nd/Sm system. In the related Nd/Pr superlattices, evaporated in similar conditions, the study of the strain and concentration profiles through the bilayer [12] has shown that the interface extends approximately over four atomic planes.

Average **c** parameters have been systematically deduced from the (004) Bragg peak positions. Figure 4 presents their variation with the ratio of the layer thicknesses. The theoretical values of the **a** and **c** parameters determined from an ideal elastic model are also reported in the same figure. In such a model, a superlattice is considered as the pseudomorphic stacking of Nd and Sm layers with equal values of the in-plane **a** parameters for both metals; the crystal parameters are then obtained by minimizing the total elastic energy of the system with respect to the strains [19]. The result of the calculation shows that, when the relative Nd thickness increases, the value of the **a** parameter continuously increases from its value in thick dhcp Sm films towards its value in bulk Nd. Simultaneously, the **c** parameters decrease in both Sm and Nd layers. Thus the calculated value of the average **c** parameter increases with the ratio Nd layers thickness/Sm layers thickness. The experimental variation of **c** parameter is in very good agreement with the values deduced from the simple ideal elastic model.

4. Magnetic properties

The magnetic structures of dhcp Nd and Sm are recalled first. Below 19.9 K, Nd forms a longitudinally modulated magnetic structure involving moments on the hexagonal sites [20]. The moments are along the **a**-direction in the basal plane and successive hexagonal planes order antiferromagnetically. Below 19.1 K, the moments tilt away from the **a**-direction to give a 2-**Q** structure [21]. Further modulated structures occur below 8.3 K corresponding to the onset of order on the cubic sites. At low temperature, the cubic sites also exhibit a 2-**Q** structure, locked in a specific orientation relatively to the 2-**Q** structure of the hexagonal sites [22]. In dhcp Sm, the hexagonal and cubic sublattices both order magnetically below 25 K, with moments along the **c**-direction [23]. Both phases present an antiparallel arrangement along **c**, with either ferro- or antiferro-magnetic basal plane coupling for the hexagonal and cubic sublattices, respectively (propagation vector (001) and (0.25, 0, 1)).

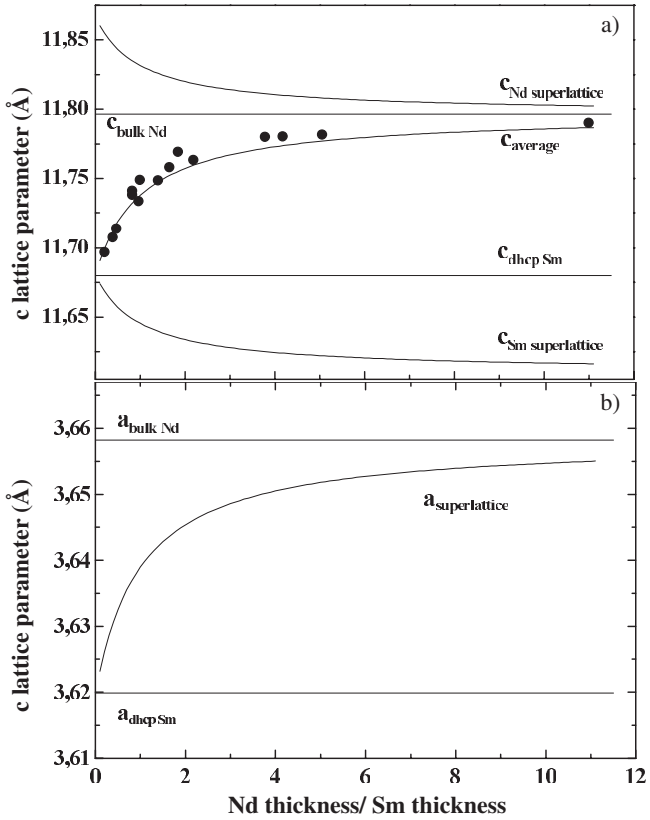

Figure 4. Variation of the lattice parameters as a function of the ratio: Nd layers thickness/Sm layers thickness. The continuous lines result from theoretical calculations (see text). The full circles are the measured average **c** parameters.

The magnetic structures in Nd/Sm superlattices change drastically with the superlattice composition. In the following, the RXMS results for superlattices with thicker Sm layers and with thicker Nd layers will be discussed separately.

4.1. Samples with thicker Sm layers: $[Nd(3.7\ nm)/Sm(9.4\ nm)]_{43}$ *and* $[Nd(7.1\ nm)/Sm(8.7\ nm)]_{33}$

4.1.1. Sm magnetic order. The study of Sm magnetism has been performed at the Sm L_{III} edge. For both superlattices, below 25 K, several magnetic reflections have been observed at positions $\mathbf{Q} = (00L)$ and (0.25, 0, L), with L close to 3, 5, 7 and 9 rlu, and are attributed to long-range magnetic order in the hexagonal and cubic sublattices, respectively, like in dhcp Sm films [23].

We first need to stress that the rlu is defined by using the average **c** lattice constant ($\mathbf{c}_{average}$) at low temperature. At resonance, we are sensitive only to one of the constituents of the superlattice, and the positions of the magnetic peaks result from the convolution of the magnetic Bragg peak with the superlattice delta function. In Sm layers, the lattice **c** parameter parallel to the growth direction is $\mathbf{c}_{Sm} < \mathbf{c}_{average}$ (see figure 4, at room temperature). As a consequence, in figures 5 and 6, the values of L in rlu, for which magnetic peaks corresponding to Sm

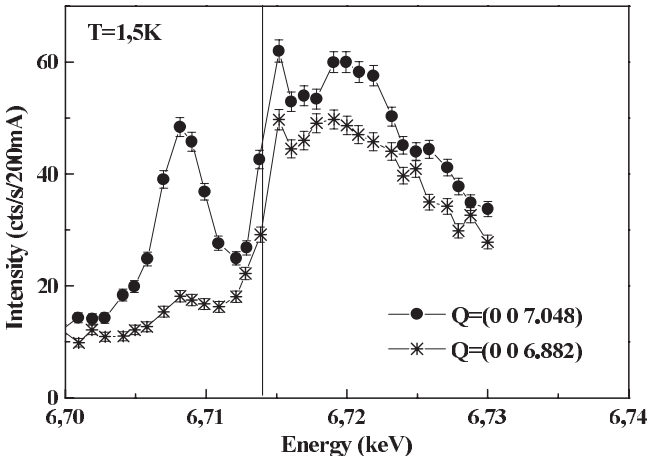

Figure 5. Energy dependence at 1.5 K at (0,0,7.048) (magnetic peak, full circles) and at (0,0,6.88) (far away from any magnetic reflection, stars) for $[\mathrm{Nd}(3.7\ \mathrm{nm})/\mathrm{Sm}(9.4\ \mathrm{nm})]_{43}$. The lines are guides to the eye. The solid vertical line indicates the position of the inflection point in the fluorescence.

hexagonal and cubic sites orders are observed, are not integers. The remark also applies to magnetic phases of the Nd layers where the lattice parameter is $\mathbf{c}_{\mathrm{Nd}} > \mathbf{c}_{\mathrm{average}}$ (see figure 4).

In both samples with thicker Sm layers, the energy dependence of the intensity at positions in reciprocal space corresponding to the ordering of the hexagonal and cubic sublattices present the same features, illustrated in figure 5, for the $[\mathrm{Nd}(3.7\ \mathrm{nm})/\mathrm{Sm}(9.4\ \mathrm{nm})]_{43}$ sample. The energy dependence at the magnetic Bragg position $\mathbf{Q} = (0, 0, 7.048)$ exhibits a well-resolved peak at 6.708 keV, 6 eV below the edge (defined as the position of the inflection point in the fluorescence). This peak is absent from the measurement at $\mathbf{Q} = (0, 0, 6.88)$, far away from any magnetic reflection, and is attributed to quadrupolar $2\mathrm{p} \rightarrow 4\mathrm{f}$ transitions. Above the edge, the observed broad feature is present at all scattering vectors and can be attributed to the tail of the fluorescence signal: no clear signature of dipolar $2\mathrm{p} \rightarrow 5\mathrm{d}$ transitions is evidenced. Similar energy dependence has also been observed in thick dhcp Sm films [23]. In the following, **Q**-scans have been performed at fixed incident photon energy, 6.708 keV, and thus reflect the behaviours of the Sm 4f moments.

We have studied the propagation of the magnetic order in the growth direction of the Sm hexagonal and cubic sublattices through the Nd layer by performing scans in reciprocal space, along the $[00L]$ and $[0.25, 0, L]$ directions, respectively (figure 6). In the case of the hexagonal sublattice (figures 6(a) and (b)), equivalent scans at a photon energy of 6.7 keV, away from the resonance, reflect the charge background.

Let us first consider the Sm hexagonal sublattice. For $[\mathrm{Nd}(3.7\ \mathrm{nm})/\mathrm{Sm}(9.4\ \mathrm{nm})]_{43}$ (figure 6(a)), a single magnetic peak is observed at the resonance at $\mathbf{Q} = (0, 0, 7.048)$ while it is missing at 6.7 keV. Its width, corrected for instrumental resolution, reflects a coherent propagation of the magnetic structure through three superlattice periods. Note the absence of magnetic superlattice peaks. This is surprising since the observation of structural (figure 2) as well as magnetic (figure 6(c), cubic sublattice) superlattice peaks in the same sample warrants the quality of the superperiodicity. This lack of magnetic superlattice peaks could indicate that a similar order is induced in the Nd layer. However this hypothesis has to be eliminated because:

(i) we fail to observe such an order in the Nd layers (see next section), and

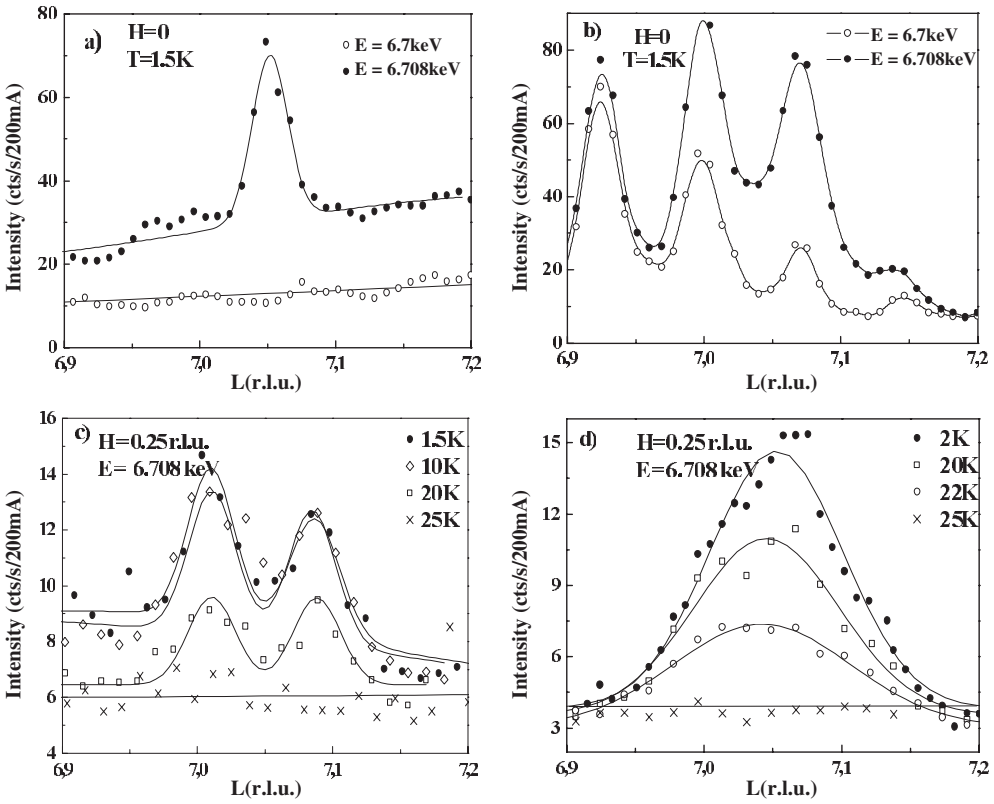

Figure 6. Scan in the **c***-direction at the samarium L_{III} edge, for the superlattices with thick Sm layers, $[Nd(3.7\ nm)/Sm(9.4\ nm)]_{43}$ (left) and $[Nd(7.1\ nm)/Sm(8.7\ nm)]_{33}$ (right), at positions corresponding to the long-range magnetic order in the hexagonal (top) and cubic (bottom) sublattices. In (a) and (b), the equivalent scan at 6.7 keV (away from the resonance) reflects the charge background.

(ii) the values of the magnetic moments of Sm and Nd are very different: even in the case of a similar structure, the magnetic contrast should be strong.

For $[Nd(7.1\ nm)/Sm(8.7\ nm)]_{33}$ (figure 6(b)), the spectra measured at the resonance and at 6.7 keV, around $\mathbf{Q} = (007)$, both present a series of peaks separated by $2\pi/\Lambda$, Λ being the superlattice repeat. They are attributed to leakage from the un-rotated polarization channel, where they have intensities several orders of magnitude higher and are due to the structure of the superlattice. Nevertheless, the resonant spectrum exhibits an additional broad contribution around 7.05 rlu, with approximately a 0.1 rlu width (figure 6(b)). Such a width corresponds to a magnetic coherence length close to one Sm layer thickness. We have checked its magnetic origin by studying its energy dependence: the resonance at 6.708 keV is clearly observed, with a line shape similar to that presented in figure 5.

Let us now detail the magnetic behaviour of the Sm cubic sublattice. For $[Nd(3.7\ nm)/Sm(9.4\ nm)]_{43}$, below 25 K, two magnetic peaks, separated by $2\pi/\Lambda$, are evidenced (figure 6(c)). Their widths show that the cubic sites' magnetic order propagates coherently over 28 nm (approximately two superperiods).

In contrast, for $[Nd(7.1\ nm)/Sm(8.7\ nm)]_{33}$, a single broad peak is observed below 25 K (figure 6(d)). Its width increases with temperature and corresponds to a magnetic coherence

length decreasing from 10 nm (approximately one single Sm layer thickness) at 2 K to 7 nm just below 25 K.

To summarize, in superlattices with large Sm thickness (9.4 and 8.7 nm), the magnetic phases in Sm layers are similar to the ones in dhcp thick films. Both magnetic orders in the hexagonal and cubic sublattices propagate coherently through Nd when the Nd thickness is 3.7 nm. Both are confined in individual Sm layers when the Nd thickness is 7.1 nm.

4.1.2. Nd magnetic order. Despite extensive searches at low temperature, no magnetic scattering was detected at the Nd L_{III} edge in $[Nd(3.7\ nm)/Sm(9.4\ nm)]_{43}$, either for the magnetic wavevectors associated to Nd order or for those associated to the dhcp Sm order. Likewise, in $[Nd(7.1\ nm)/Sm(8.7\ nm)]_{33}$, a more partial study did not reveal any Nd magnetic order.

The Nd L_{II} edge (6.722 keV) being only 6 eV above the Sm L_{III} edge (6.716 keV), the search was performed at the Nd L_{III} edge (6.208 keV), shown later in superlattices with thick Nd layers to give resonant intensities about an order of magnitude smaller (see the next section). The fact that no magnetic signal was detected can be attributed either to its weakness, or to the fact that the magnetic structure is different from both the Sm and Nd magnetic structures, or finally to the lack of Nd magnetic ordering, as already reported in Ce/Nd superlattices [14]. This will be further discussed in section 5.

4.2. Samples with thicker Nd layers: $[Nd(18.8\ nm)/Sm(3.7\ nm)]_{42}$, $[Nd(15.4\ nm)/Sm(1.4\ nm)]_{47}$ *and* $[Nd(6.2\ nm)/Sm(3.7\ nm)]_{84}$

4.2.1. Nd magnetic order. In the three Nd/Sm superlattices with thick Nd layers, several magnetic reflections at positions close to (0.13, 0, L), with $L = 3$, 5, 7 and 9 rlu have been evidenced below 19 K. The positions of these magnetic peaks correspond to incommensurate order of the hexagonal sublattice in bulk Nd. The measured resonant intensity at these positions was about one order of magnitude higher at the L_{II} edge than at the L_{III} edge. The full study was then performed at the Nd L_{II} edge, despite its closeness to the L_{III} Sm edge, as the splitting between the resonances has been proved to be sufficient to separate them unambiguously.

At 8 K, additional magnetic peaks appear, at positions close to (0.18, 0, L), corresponding to cubic sites ordering in bulk Nd.

In all three samples, the energy dependences of the magnetic intensities associated with the magnetic order in the Nd hexagonal and cubic sublattices are similar, with a dipole resonance at 6.723 keV. As an example, figure 7 presents the energy dependence of the intensity at (0.124, 0, 7) at 6 K for $[Nd(18.8\ nm)/Sm(3.7\ nm)]_{42}$. A resonance is observed at 6.723 keV, close to the dipole transition. As generally observed at the L_{II} edge for rare-earth metals, there is no clear signature of a quadrupole resonance [24].

The Nd ordering was then studied at the maximum of the resonance, 6.723 keV, where the resonant intensities reflect the polarization of the Nd 5d band.

As an illustration of the behaviour of the superlattices with thicker Nd layers, the temperature dependence of the Nd magnetic scattering in $[Nd(18.8\ nm)/Sm(3.7\ nm)]_{42}$ is summarized in figures 8 and 9. Figure 8 shows scans along (H07) at different temperatures between 19 and 2 K. Below 19 K, the peak attributed to the Nd hexagonal sites appears at $H = 0.138$ rlu (labelled hexagonal in figures 8 and 9). We verify that, like in bulk Nd, this peak is actually slightly split in the in-plane direction perpendicular to $\mathbf{a}^*$, as a result of the 2-$\mathbf{Q}$ magnetic structure, where the coupled propagation vectors have a small in-plane component perpendicular to $\mathbf{a}^*$. Figure 9 presents the thermal variation of the component of: (i) the magnetic propagation vector along $\mathbf{a}^*$, (ii) the in-plane magnetic coherence lengths, and (iii) the

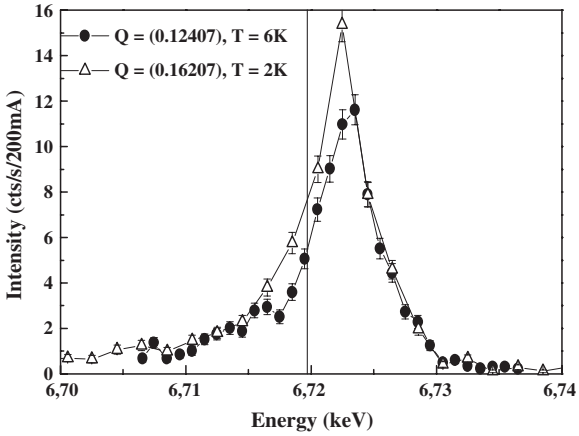

Figure 7. Energy dependence of the resonance at the Nd L_{II} edge for the $[Nd(18.8\ nm)/Sm(3.7\ nm)]_{42}$ superlattice, at positions $\mathbf{Q} = (0.124,0,7)$ at 6 K (full circles, hexagonal sublattice) and $\mathbf{Q} = (0.162,0,7)$ at 2 K (open triangles, new magnetic phase, see text). The lines are guides to the eye. The solid vertical line indicates the position of the inflection point in the fluorescence.

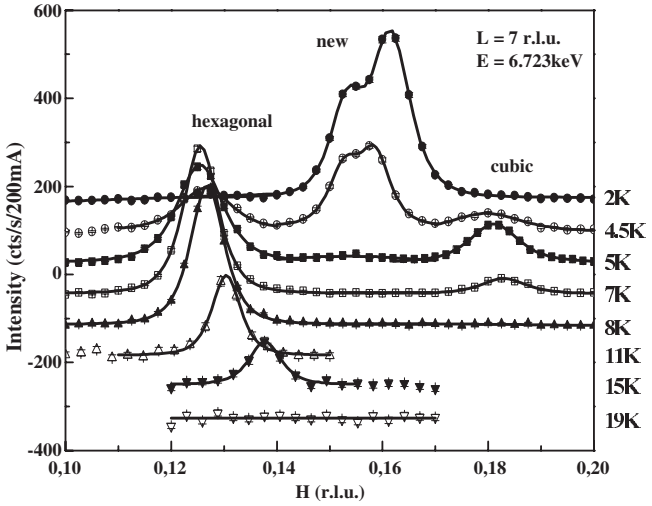

Figure 8. RXMS intensity at the Nd L_{II} dipole resonance for $\mathbf{Q} = (H\ 07)$ at various temperatures for $[Nd(18.8\ nm)/Sm(3.7\ nm)]_{42}$. The curves have been offset vertically for clarity.

integrated intensities determined from the magnetic peaks shown in figure 8. Between 19 and 6 K, the thermal variation of the in-plane component of the magnetic propagation vector is very close to the bulk Nd one (figure 9(a)). However, the H-values are slightly larger than the bulk ones. Contrarily to what is observed in bulk Nd, no splitting along $\mathbf{a}^*$ is observed at 6 K (figure 9(a)); however, the value of H increases below this temperature.

Below 8 K, the magnetic peak attributed to the cubic sites in bulk Nd is observed at $H = 0.181$ rlu (labelled cubic in figures 8 and 9). Between 8 and 5 K, the H-values are slightly smaller than the bulk ones (figure 9(a)).

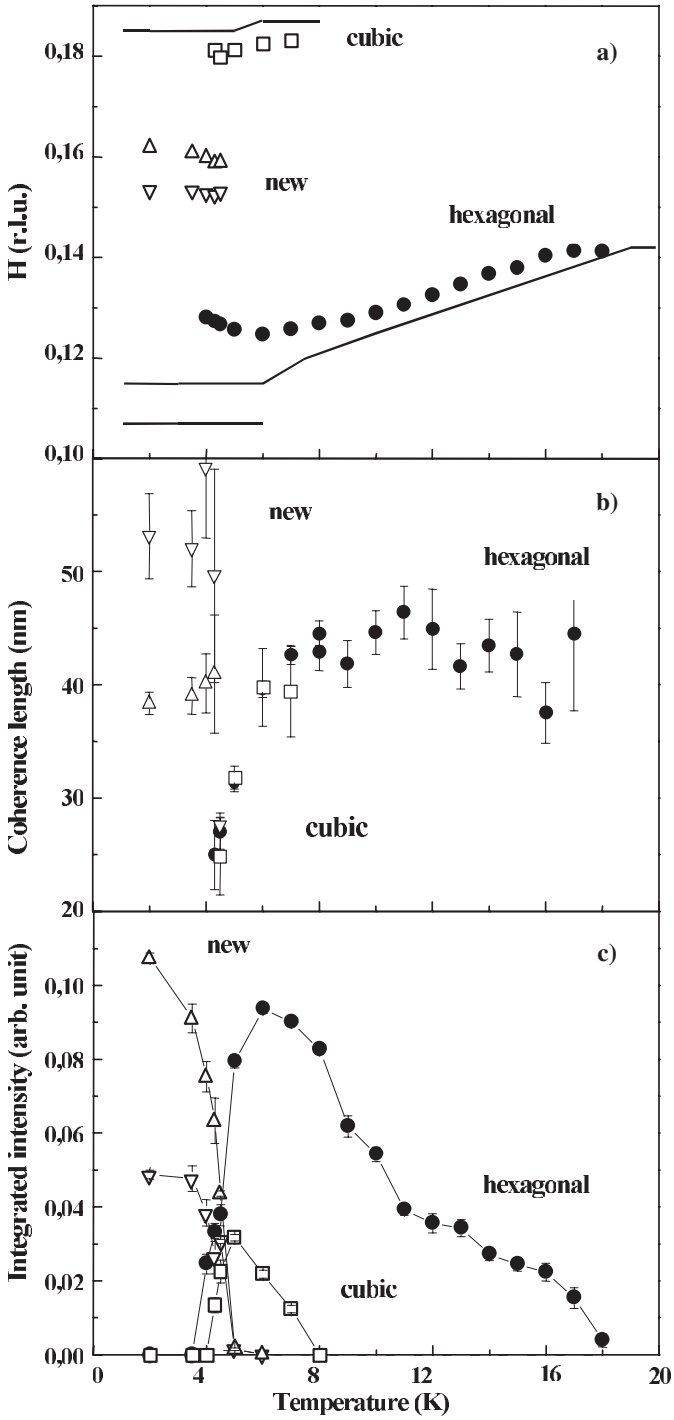

Figure 9. Thermal variation of the H positions (a), in-plane coherence length (b) and integrated intensities (c) of the magnetic peaks attributed to the ordering of the Nd hexagonal sites (full circles), of the Nd cubic sites (squares) and of the new low-temperature phase (up and down triangles) for $[Nd(18.8\ nm)/Sm(3.7\ nm)]_{42}$ at the Nd L_{II} dipolar resonance. The continuous lines in figure 8(a) are the bulk values [17].

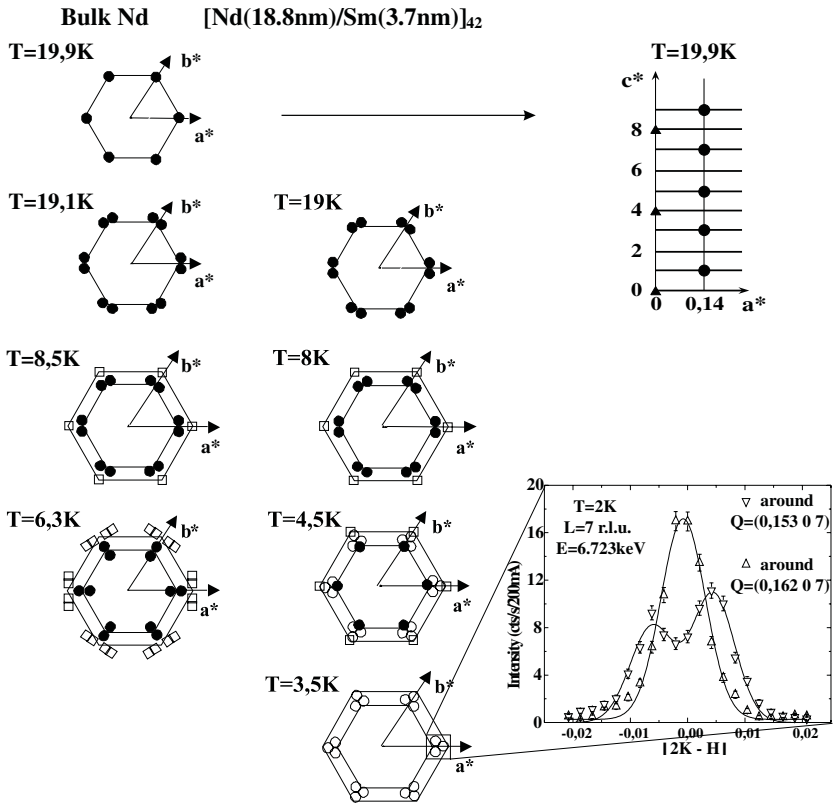

Figure 10. Projections of the magnetic propagation vectors onto the ($\mathbf{a}^*$, $\mathbf{b}^*$) reciprocal plane around $\mathbf{Q} = (007)$ at different temperatures for bulk Nd (left column) and for $[\mathrm{Nd}(18.8\ \mathrm{nm})/\mathrm{Sm}(3.7\ \mathrm{nm})]_{42}$ (right column): hexagonal sites order (filled circles), cubic sites order (squares) and new magnetic phase order (empty circles). Top inset: positions of the structural (triangles) and magnetic (circles) peaks in the ($\mathbf{a}^*$, $\mathbf{c}^*$) reciprocal plane at 19.9 K for bulk Nd. Bottom inset: RXMS intensity at the Nd dipolar resonance along the 2**K**–**H**-direction around $\mathbf{Q} = (0.153,0,7)$ (down triangles) and $\mathbf{Q} = (0.162,0,7)$ (up triangles) at 2 K for $[\mathrm{Nd}(18.8\ \mathrm{nm})/\mathrm{Sm}(3.7\ \mathrm{nm})]_{42}$.

The in-plane magnetic coherence length of the magnetic phase attributed to the cubic sites is very close to that of the hexagonal sites, both of them decreasing simultaneously with temperature below 8 K (figure 9(b)).

More surprising are the observations below 5 K, where the behaviour deviates drastically from the bulk one. The intensities of the peaks attributed to the magnetic order of the hexagonal and cubic sublattices decrease rapidly, and vanish at 3.5 and 4 K, respectively. Simultaneously, new peaks appear at 4.5 K at intermediate H-values: $H = 0.1525$ rlu and $H = 0.162$ rlu (labelled as new (new magnetic phase) in figures 8 and 9). Their intensities increase on cooling down to 1.5 K, while the associated positions (figure 9(a)) and in-plane magnetic coherence length (figure 9(b)) present very small variations.

Scans performed at 2 K along the in-plane direction perpendicular to $\mathbf{a}^*$ (2**H**–**K**) across the two magnetic contributions are presented in the inset of figure 10. The scan measured around (0.153,0,7) shows a splitting in this direction, with two maxima symmetric with respect to the $\mathbf{a}^*$-direction, like in the 2-**Q** magnetic structure of the hexagonal sublattice. No splitting is observed around the (0.162,0,7) peak, like in the cubic sublattice above 4.5 K.

The energy dependence at 2 K of the (0.162, 0, 7) magnetic reflection is presented in figure 7 together with the energy dependence of the intensity at (0.124, 0, 7). The apparent shift, as compared to the resonance observed may be simply due to interference effects with the non-resonant magnetic scattering (low-energy tail), although a more detailed study, based on the measurement of integrated intensities would be needed to conclude on that point. To summarize, figure 10 presents the projections of the magnetic propagation vectors in the ($\mathbf{a}^*$, $\mathbf{b}^*$) plane at different temperatures for bulk Nd [21] and for $[Nd(18.8\ nm)/Sm(3.7\ nm)]_{42}$. By analogy with the results obtained in bulk Nd between 8 and 6 K [21], the new phase observed in our superlattice may be considered as 3-**Q** phase, resulting from the coupling between a 2-**Q** phase in the hexagonal sublattice, and a single **Q** phase in the cubic sublattice. Such an assertion is consistent with the discussion of Forgan *et al* [22] on the low-temperature magnetic structure in bulk Nd.

Very similar results have been observed in $[Nd(6.2\ nm)/Sm(3.7\ nm)]_{84}$ and in $[Nd(15.4\ nm)/Sm(1.4\ nm)]_{47}$. In these samples, the new magnetic peaks observed at low temperature are located at $H = 0.157$ and 0.163 rlu and at $H = 0.154$ and 0.166 rlu, respectively. In $[Nd(6.2\ nm)/Sm(3.7\ nm)]_{84}$, this low-temperature phase has also been observed by neutron scattering, which shows that, although the dipole Nd L_{II} resonance only gives access to the polarization of the 5d band, it actually reflects the magnetic order of the 4f moments in these structures.

The scattering observed when **Q** is scanned in the $\mathbf{c}^*$-direction across the above magnetic satellites gives information on the propagation of the Nd magnetic order in the growth direction through Sm layers. In $[Nd(18.8\ nm)/Sm(3.7\ nm)]_{42}$, for the hexagonal sublattice and the new phase, two magnetic peaks separated by $2\pi/\Lambda$ are evidenced (figures 11(a) and (b)). The coherence lengths deduced from their widths are $\approx$76 and 60 nm, respectively, which shows that these magnetic structures propagate coherently through the Sm layers. In contrast, a single broad peak is observed for the cubic sublattice with a coherence length of $\approx$17 nm, showing that the order of the cubic sublattice is confined to individual Nd layers (figure 11(c)).

Similar results are observed for the $[Nd(6.2\ nm)/Sm(3.7\ nm)]_{84}$ superlattice. However, in $[Nd(15.4\ nm)/Sm(1.4\ nm)]_{47}$, coherence through the Sm layers is also observed for the magnetic order in the cubic sublattice, with a coherence length of 67 nm (more than 5 superlattice periods, figure 12). Such a coherence of the Nd cubic sites order has never been observed in Nd-based superlattices and will be discussed in section 5.

4.2.2. Sm magnetic order. The study of Sm magnetism has been performed at the Sm L_{III} edge. It was unfortunately impossible to measure any magnetic contribution from the ordering on the hexagonal sites, because of the superimposition of charge scattering from the lattice and because of the weakness of the expected magnetic signal due to small Sm relative thickness.

However, the magnetic satellites corresponding to the magnetic ordering of the moments located on the cubic sites could be extracted. As in pure dhcp films [23] and in superlattice with a thick Sm layer (figure 5), a clear resonance is observed below the edge ($E = 6.708$ keV) and is attributed to quadrupole transitions. The ordering temperature is close to 24 K. The magnetic propagation vector is again (0.25, 0, 1) and does not change with temperature. This characterizes a magnetic phase commensurate with the crystal lattice. Scans along $\mathbf{a}^*$ around the (0.25, 0, 7) peak are presented in figure 13 for $[Nd(18.8\ nm)/Sm(3.7\ nm)]_{42}$. Contrarily to what is observed in Nd/Sm with thick Sm layers (figures 6(c) and (d)), the intensity of the peak dramatically decreases at low temperature. The in-plane magnetic coherence length of the magnetic phase attributed to the Sm cubic sites is 45 nm at 17 K and decreases to reach 25 nm at 5 K.

Scans in the $\mathbf{c}^*$-direction are very broad. The magnetic coherence length is shorter than the thickness of the individual Sm layers and the Sm magnetic order is confined in the Sm layers.

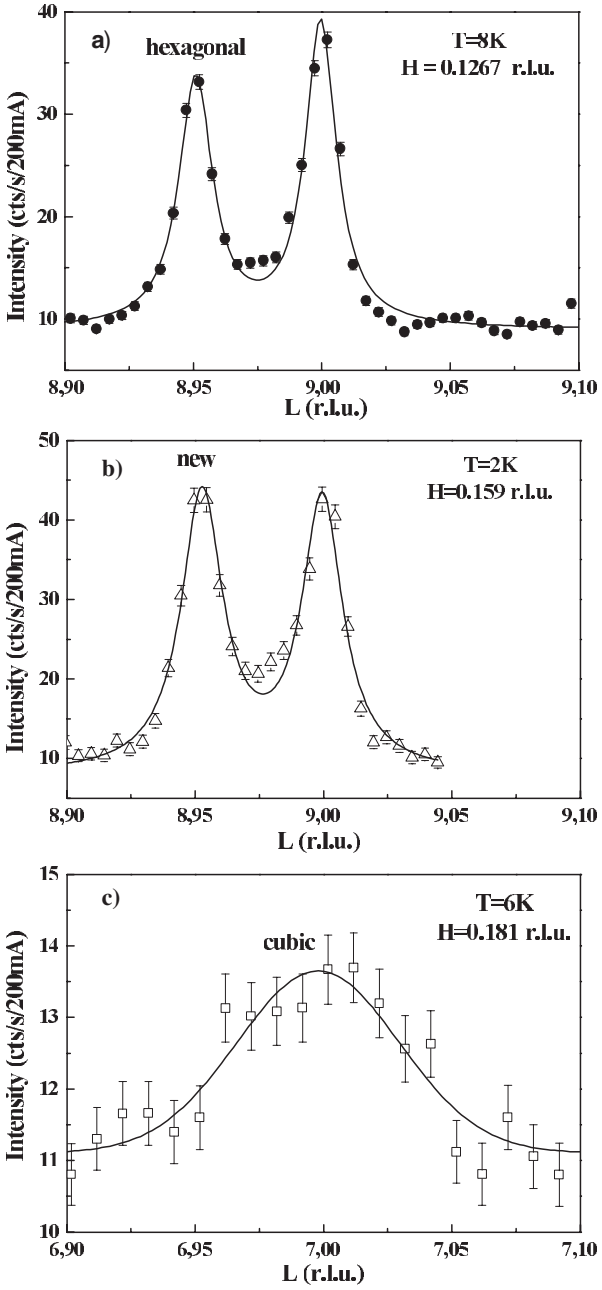

Figure 11. Scans in the **c***-direction at the Nd L_{II} dipolar resonance through magnetic reflections attributed to the hexagonal (a) and cubic (c) sites ordering above 5 K and to the new magnetic ordering (b) below 5 K for $[Sm(3.7\ nm/Nd(18.8\ nm)]_{42}$. Scans in the **c***-direction performed for $H = 0.153$ and 0.162 rlu on another diffractometer with a different resolution are not presented here; they present the same features as the scan shown in (b).

Similar results are observed for the $[Nd(6.2\ nm)/Sm(3.7\ nm)]_{84}$ superlattice. However, it is of note that no magnetic signal could be extracted at the L_{III} Sm edge for the superlattice with

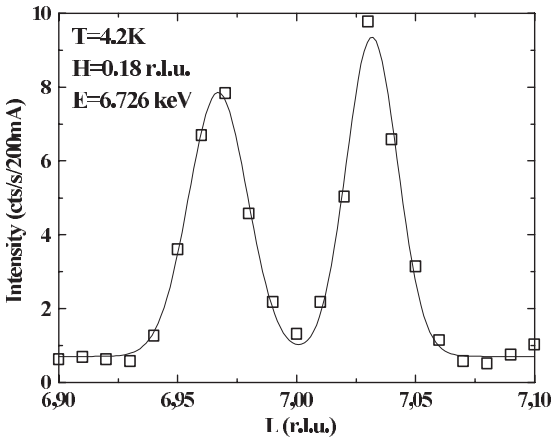

Figure 12. Scan in the **c***-direction at the Nd L_{II} dipolar resonance through magnetic reflections attributed to cubic site ordering at 5 K for $[Sm(1.4\ nm/Nd(14.4\ nm)]_{47}$.

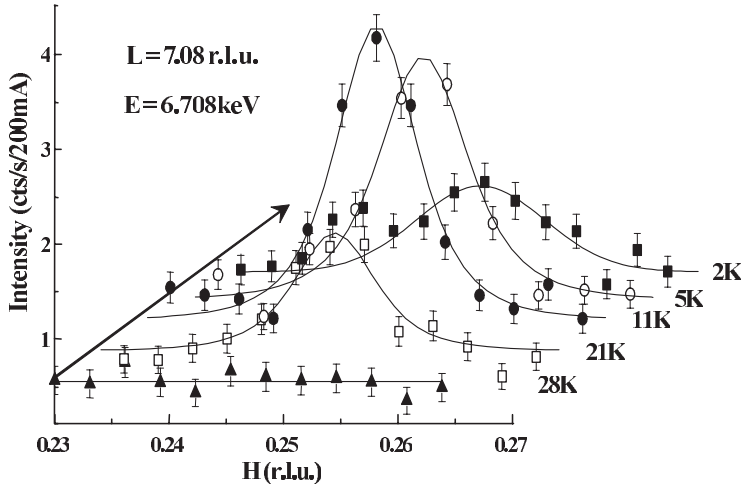

Figure 13. RXMS intensity at the Sm L_{III} quadrupolar resonance for $\mathbf{Q} = (\mathbf{H},0,7.08)$ at various temperatures for $[Nd(18.8\ nm)/Sm(3.7\ nm)]_{42}$.

the thin Sm layers (1.4 nm). This absence of magnetic signal can be attributed to its weakness or to the lack of magnetic ordering.

5. Discussion

Table 2 summarizes the experimental results described in section 4 and discussed in this section.

5.1. Magnetic phases in Nd/Sm superlattices

Concerning the magnetic phases of the Sm layers, the experimental results can be summarized as follows.

(i) In superlattices with thick Sm layers (9.4 and 8.7 nm), both magnetic phases associated to hexagonal and cubic sites ordering are observed.

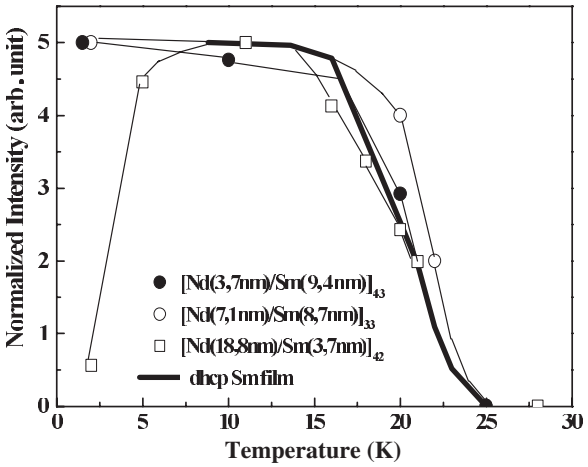

Figure 14. Thermal variation of the magnetic intensities attributed to the Sm cubic site ordering in: (a) a thick Sm film (bold line); (b) [Nd(3.7 nm)/Sm(9.4 nm)]$_{43}$ (filled circles); (c) [Nd(7.1 nm)/Sm(8.7 nm)]$_{33}$ (empty circles) and (d) [Nd(18.8 nm)/Sm(3.7 nm)]$_{42}$ (squares).

Table 2. Occurrence and coherence of the magnetic phases observed in the Nd/Sm superlattices: C: coherent magnetic phase; NC: non-coherent magnetic phase; NM: no magnetic order; No obs: magnetic phases probably not observed because of charge leak or low signal.

	Nd hexagonal	Nd cubic	Nd new phase	Sm hexagonal	Sm cubic
[Nd(3.7 nm)/Sm(9.4 nm)]$_{43}$	NM	NM	NM	C	C
[Nd(7.1 nm)/Sm(8.7 nm)]$_{33}$	NM	NM	NM	NC	NC
[Nd(18.8 nm)/Sm(3.7 nm)]$_{42}$	C	NC	C	No obs.	NC
[Nd(6.2 nm)/Sm(3.7 nm)]$_{84}$	C	NC	C	No obs.	NC
[Nd(15.4 nm)/Sm(1.4 nm)]$_{43}$	C	C	C	No obs.	No obs.

(ii) In superlattices with intermediate Sm layer thickness (3.7 nm), the phase associated to hexagonal sites has not been observed due to the high charge background along [00L].

(iii) In the superlattice with the thin Sm layer (1.4 nm), no magnetic signal was evidenced at the Sm edge. It is impossible to conclude whether this absence of magnetic signal is due to its weakness or to a lack of magnetic ordering.

When observed, the magnetic phases in the Sm layers are very similar to the those in dhcp Sm thick films: they exhibit the same magnetic propagation vector and the same ordering temperature as thick dhcp films.

Figure 14 summarizes the thermal evolution of the magnetic intensity for cubic sites order for a thick dhcp film (continuous line) and for several Nd/Sm superlattices. The main point is that for superlattices with thick Sm layers (9.4 and 8.7 nm), the cubic sites' magnetic order is observed down to low temperature. In contrast, for a superlattice with thinner Sm layers (3.7 nm), the intensity of the corresponding magnetic peaks exhibits a very significant decrease below 10 K. Such a decrease can be attributed either to a reorientation of the Sm magnetic moments or to a change of Sm order: either a new order takes place or Sm magnetic moments are no longer ordered. In [Nd(18.8 nm)/Sm(3.7 nm)]$_{42}$, no experimental evidence of a new magnetic phase (different from the dhcp Sm films one) has been demonstrated. More extensive searches are however necessary to make a definitive conclusion. Nevertheless, the fact that the

observed magnetic structure in the Sm cubic sublattice at low temperature disappears when the new magnetic phase with intermediate propagation vectors appears in the Nd layers shows drastic changes in the overall magnetic behaviour of this superlattice below 5 K. Further studies are still needed to fully elucidate that point.

Concerning the Nd magnetic phases, two different behaviours have been observed.

(i) In superlattices with a thick Sm layer (>8 nm), no magnetic order has been evidenced in Nd layers. In fact, in $[Nd(3.7\ nm)/Sm(9.4\ nm)]_{43}$, the Sm magnetic order propagates coherently along the **c**-axis through Nd layers and perhaps prevents the development of the Nd in-plane magnetic order.
(ii) One of the main results presented in this paper is that, in superlattices with thinner Sm layers (<4 nm), the Nd magnetic order is very different from the one observed in bulk Nd: a new magnetic phase with intermediate propagation vectors has been evidenced at low temperature.

This new Nd magnetic phase is observed when the bulk-like hexagonal and cubic sites' order disappear simultaneously. Thus, it can be attributed to both sites, and the magnetic moments located on the hexagonal and cubic sites seem to exhibit a common magnetic order. One has to note that such a modification of the wavevector value has never been observed in previously studied Nd-based superlattices (Nd/Pr, Nd/La, Nd/Ce). However, Forgan *et al* [25] observed a similar structure in bulk Nd under magnetic field. This structure presents 'two distinct wavevectors with lengths intermediate between those normally associated with the hexagonal and cubic wavevectors'. The reason for the formation of such a structure is unclear, but it almost certainly involves an interaction between the structures associated with each symmetry site and would be favoured by the application of a field (magnetic, strain, etc). A further investigation of the thermal dependence of the lattice strain in the Sm and the Nd layers would be interesting to eventually correlate a strain variation and the occurrence of the new magnetic phase. Let us stress that, surprisingly, this new Nd ordering only appears when the thickness of the Nd layers is large (>6 nm).

5.2. Propagation of the magnetic phases in Nd/Sm superlattices

In an A/B superlattice, the coherent propagation of the magnetic order of A through B is commonly achieved via the stabilization of a spin-density wave in the layers B. The main question is then whether the formation of such a spin-density wave is compatible with a magnetic order with a perpendicular polarization in B.

When considering dhcp superlattices with two non-equivalent sites, an additional issue is opened: does the magnetic coupling of the hexagonal sites differ from that of the cubic sites?

The answer to these questions is very different when considering, on one hand, the propagation of the Sm order through Nd layers and, on the other hand, the propagation of Nd order through Sm layers.

Concerning the propagation of the Sm magnetic order through Nd layers, our main result is that, in $[Nd(3.7\ nm)/Sm(9.4\ nm)]_{43}$, below 25 K, a simultaneous coherent propagation of the Sm hexagonal and cubic sites' magnetic orders through Nd layers has been shown for the first time. In contrast, both Sm hexagonal and cubic sites' magnetic orders are confined to single Sm blocks when the Nd thickness is larger (in $[Nd(7.1\ nm)/Sm(8.7\ nm)]_{43}$). The results observed in $[Nd(18.8\ nm)/Sm(3.7\ nm)]_{42}$ and in $[Nd(6.2\ nm)/Sm(3.7\ nm)]_{84}$ are also in agreement with the previous conclusion. The Sm cubic sites' magnetic phase does not propagate through 6.2 and 18.8 nm Nd layers. However, in these samples, the hexagonal sites' order has not been observed probably because of charge leak.

Thus, in Nd/Sm superlattices, the Nd critical thickness for a coherent propagation of both Sm hexagonal and cubic sites' order is comprised between 3.7 and 6.2 nm. This critical value is smaller than the one measured in other rare earth superlattices (around 10 nm in Dy/Y for example).

Concerning now the propagation of Nd magnetic order through Sm layers: in $[Nd(18.8\ nm)/Sm(3.7\ nm)]_{42}$ and in $[Nd(6.2\ nm)/Sm(3.7\ nm)]_{84}$, both the hexagonal sites' order (between 19 and 5 K) and the new magnetic order (below 5 K) propagate coherently through several bilayers whereas the cubic sites' order (between 8 and 5 K) remains confined in the Nd layers. Because of the relatively small thickness of Sm layers (3.7 nm) in these samples, the lack of coherence of Nd cubic sites' magnetic order is surprising. However, as mentioned in the introduction, similar results have been obtained in Nd/Pr and Nd/La superlattices where the thickness of the spacer layer is approximately equal to 3 nm (La) or 9.8 nm (Pr). In contrast, in $[Nd(15.4\ nm)/Sm(1.4\ nm)]_{47}$, all the Nd magnetic phases (including the cubic sites' one between 8 and 5 K) propagate coherently through Sm layers.

Thus, above 5 K, the critical thicknesses of Sm layers below which a coherent propagation of the Nd order occurs are different for the hexagonal and cubic sites. For Nd hexagonal sites' order, it is larger than 3.7 nm. For cubic sites' order, it is comprised between 1.4 and 3.7 nm.

To explain the lack of coherent magnetic propagation, one has to consider the generalized susceptibility of the conduction electrons. Experimental data are not available for Nd metal but only for Pr metal. When Pr orders, its magnetic structure closely resembles that of Nd; thus, one can conclude that they have similar Fermi surfaces and magnetic excitations spectra. The measured magnetic excitation spectra for Pr metal provide evidence for a susceptibility of the conduction electrons that is large for an antiferromagnetic configuration of the hexagonal layers and small for cubic sites' ordering [26]. In fact, from Houmann *et al* [27], the excitations propagating along the **c**-direction on the cubic sites have negligible dispersion, in contrast to those on the hexagonal sites, indicating that the total coupling between different layers of cubic ions is very small. In conclusion, by analogy with Pr, different values of the susceptibility of the conduction electron can explain the different magnetic coherence lengths for Nd hexagonal and cubic sites in Nd-based superlattices. In contrast, in dhcp Sm, generalized susceptibilities of the conduction electrons on the hexagonal and cubic sites could present values of the same order of magnitude. Such an assertion is suggested by the similar ordering temperature of both types of site in dhcp Sm. This would explain the simultaneous coherent propagation of Sm hexagonal and cubic sites' magnetic order observed in $[Nd(3.7\ nm)/Sm(9.4\ nm)]_{43}$.

The above discussion underlines the fact that, when the hexagonal and cubic sites' magnetic orders present different propagation vectors, their propagations are independent phenomena, because different parts of the Fermi surface are responsible for these propagations.

We are now going to comment on the coexistence of magnetic orders with competing anisotropies. According to Simpson *et al*, in Ho/Er superlattices [9], an in-plane magnetic order and a **c**-axis one arise from different states of the conduction electrons at the Fermi surface. Because it is not possible to match these states at the interface, the conduction electrons in the in-plane ordered state cannot transmit the **c**-axis information. In consequence, there is no coherence of the Er longitudinal moments between Er blocks.

Our study suggests that in Nd/Sm dhcp superlattices:

- the establishment of a spin-density wave and a 4f magnetic order with perpendicular polarization is not favourable *on a given crystallographic site* (hexagonal or cubic). Such an assertion is suggested by the lack of Nd (respectively Sm) magnetic ordering observed in $[Nd(3.7\ nm)/Sm(9.4\ nm)]_{43}$ (respectively in $[Nd(15.4\ nm)/Sm(1.4\ nm)]_{43}$). This assertion is consistent with the results in hcp heavy rare-earth superlattices (Ho/Er, Dy/Er, Ho/Tm, etc);

- a 4f magnetic order *on a site with a given symmetry* does not perturb the establishment of a spin-density wave with a perpendicular polarization *on the other site with different symmetry*. As an example, in $[Nd(18.8\ nm)/Sm(3.7\ nm)]_{42}$, in Sm layers, the ordering of the Sm cubic moments does not perturb the spin-density wave correlated to coherent Nd hexagonal sites' order. Thus, either the hexagonal and cubic sites are completely independent because of their different symmetry, or a reorientation of the magnetic moments occurs (which has to be studied in a further experiment).

6. Conclusion

We have successfully stabilized dhcp Sm in the context of epitaxial Nd/Sm superlattices, resulting in a coherent dhcp stacking over many periods. The magnetic structure of Nd/Sm superlattices strongly depends on the relative layers thicknesses. Our results underline different Sm and Nd behaviours. When they are observed, the magnetic phases in Sm layers are very close to the ones observed in dhcp thick films. In contrast, the magnetism in Nd shows strong differences with the bulk case: either no Nd magnetic order is evidenced when the Sm layer's thickness is larger than the Nd one, or new Nd magnetic phases are observed.

Finally, we could confirm and complete the conclusion drawn from hcp superlattices with competing anisotropies, namely that 'two types of magnetic ordering cannot simultaneously establish structures which are coherent over several bilayers'. From our result on Nd/Sm superlattices (i.e. dhcp superlattices with competing anisotropies), a 4f magnetic order *on a site of a given symmetry* is exclusive with a spin-density wave with a perpendicular polarization *on the site with the same symmetry* but it does not perturb its establishment *on the site with different symmetry*. These novel exciting results bring new insight in the complex magnetism of light rare earths. Detailed information about the band structure and the Fermi surface would be of great interest to improve the understanding of this magnetism. It is hoped that the above results will stimulate theoretical contribution and experimental work using for example positron annihilation [28] in rare-earth superlattices.

Acknowledgments

We gratefully acknowledge E Lidström and N Kernavanois from the ID20 beam line and D Paul from the BM28 beamline for providing technical support during the ESRF runs in Grenoble (France).

References

[1] Vettier C, McWhan D B, Gyorgy E M, Kwo J R, Bruntschuh B M and Batterman B W 1986 *Phys. Rev. Lett.* **56** 757
[2] Cowley R A 1998 *J. Magn. Magn. Mater.* **177** 1156
[3] Erwin R W, Rhyne J J, Salomon M B, Borchers J, Sinha S, Du R, Cunningham J E and Flynn C P 1987 *Phys. Rev.* B **35** 6808
[4] Borchers J A, Salomon M B, Erwin R W, Rhyne J J, Du R R and Flynn C P 1991 *Phys. Rev.* B **43** 3123
[5] Jehan D A, McMorrow D F, Cowley R A, Ward R C C, Wells M R, Hagmann N and Clausen K N 1993 *Phys. Rev.* B **48** 5594
[6] Beach R S, Borchers J A, Matheny A, Erwin R W, Salomon M B, Everitt B, Pettit K, Rhyne J J and Flynn C P 1993 *Phys. Rev. Lett.* **70** 3502
[7] Bryn-Jacobsen C, Cowley R A, McMorrow D F, Goff J P, Ward R C C and Wells M R 1997 *Phys. Rev.* B **55** 317
[8] Dumesnil K, Dufour C, Mangin Ph, Marchal G and Hennion M 1996 *Phys. Rev.* B **54** 6407

[9] Simpson J A, Cowley R A, Jehan D A, Ward R C C, Wells M R, McMorrow D F, Clausen K N, Thurston T R and Gibbs D 1996 *Z. Phys.* B **101** 35
[10] Cowley R A, Simpson J A, Ward R C C, Wells M R and McMorrow D F 1998 *J. Phys.: Condens. Matter* **10** 2115
[11] Goff J P, Sarthour R S, McMorrow D F, Rainford B D, Wilkins C J T, Ward R C C and Wells M R 1998 *Physica* B **241** 714
[12] Goff J P, Bryn-Jacobsen C, McMorrow D F, Ward R C C and Wells M R 1997 *Phys. Rev.* B **55** 12537
[13] Goff J P, Sarthour R S, McMorrow D F, Yakhou F, Stunault A, Vigliante A, Ward R C C and Wells M R 1999 *J. Phys.: Condens. Matter* **11** L139
[14] Clegg P S, Goff J P, McIntyre G J, Ward R C C and Wells M R 2003 *Phys. Rev.* B **67** 174414
[15] Dufour C, Dumesnil K, Soriano S, Pierre D, Senet Ch and Mangin Ph 2002 *J. Cryst. Growth* **234** 447
[16] Kwo J, Hong M and Nakahara S 1986 *Appl. Phys. Lett.* **49** 319
[17] Hannon J P, Trammell G T, Blume M and Gibbs D 1988 *Phys. Rev. Lett.* **61** 1245
the authors then introduced the exchange splitting as a correction: Hannon J P, Trammell G T, Blume M and Gibbs D 1989 *Phys. Rev. Lett.* **62** 2644
[18] Lundgren E, Andersen J N, Nyholm R, Torelles X, Rius J, Delin A, Grechnev A, Eriksson O, Konvicka C, Schmid M and Varga P 2002 *Phys. Rev. Lett.* **88** 136102
[19] Dumesnil K 1995 *Thesis* INPL, Nancy, France
[20] Moon R M, Koehler W C, Sinha S K, Stassis C and Kline G R 1979 *Phys. Rev. Lett.* **43** 62
[21] Lebech B, Wolny J and Moon R M 1994 *J. Phys.: Condens. Matter* **6** 5201
[22] Forgan E M, Gibbons E P, McEwen K A and Fort D 1989 *Phys. Rev. Lett.* **62** 470
[23] Dufour C, Dumesnil K, Soriano S, Mangin Ph, Brown P J, Stunault A and Bernhoeft N 2002 *Phys. Rev.* B **66** 94428
[24] Giorgetti C, Dartyge E, Baudelet F and Brouder Ch 2001 *Appl. Phys.* A **73** 703
[25] Forgan E M, Gibbons E P, Lee S L, Zochowski S, McEwen K A and Marshall W G 1992 *J. Magn. Magn. Mater.* **104–107** 911
[26] Jensen J and MacIntosh A R 1991 *Rare Earth Magnetism* (New York: Oxford University Press)
[27] Houmann J G, Rainford B D, Jensen J and MacIntosh A R 1979 *Phys. Rev.* B **20** 1105
[28] Fretwell H E, Dugdale S B, Alam M A, Hedley D C R and Rodriguez-Gonzalez A 1999 *Phys. Rev. Lett.* **82** 3867